Contrib Mineral Petrol (1985) 90:353–366

Contributions to Mineralogy and Petrology

Genesis of acid/basic rock associations: a case study The Kallithea intrusive complex, Samos, Greece

Klaus Mezger[1,4], Rainer Altherr[2], Martin Okrusch[1], Friedhelm Henjes-Kunst[2], and Hans Kreuzer[3]

[1] Mineralogisches Institut der Universität Würzburg, Am Hubland, D-8700 Würzburg, Federal Republic of Germany
[2] Institut für Petrographie und Geochemie der Universität Karlsruhe (TH), Kaiserstraße 12, D-7500 Karlsruhe, Federal Republic of Germany
[3] Bundesanstalt für Geowissenschaften und Rohstoffe, Postfach 510153, D-3000 Hannover 51, Federal Republic of Germany
[4] *Present address:* Department of Earth and Space Sciences, SUNY at Stony Brook, NY 11794, USA

Abstract. The Kallithea intrusive complex on Samos forms part of the Miocene granitoid province of the central Aegean. The complex consists of numerous composite dikes consisting of different I-type diorites, monzodiorites, (quartz) monzonites, granodiorites, and granites, as well as rare pegmatites. Within individual dikes the different rock types display various structural relationships to each other, most of which indicate that multiple intrusion was the main process responsible for the association of different rock types. Petrographical, geochemical, and Sr isotope data prove that at least some of the different magma pulses were genetically unrelated. For others, a comagmatic relationship cannot be excluded. The most spectacular feature of the composite dikes are net-veined parts in which spherical (pillow-like) to angular bodies of microdiorite are surrounded by a network of more felsic rocks of varying compositions (monzonites, granodiorites, and monzogranites). – For the microdiorite/monzogranite pairs, a formation by unmixing due to liquid immiscibility is suggested by the following facts: (a) the presence of monzogranite ocelli within the microdiorite bodies, (b) similar compositions of those minerals present in both the basic and felsic parts, (c) the enrichment of HFS elements in the basic parts and the depletion of these elements in the acid parts, (d) similar Sr isotope initial ratios. Such an origin, however, is excluded for the other net-veined parts having felsic veins of either monzonitic or granodioritic compositions. In these pairs, the HFS elements are enriched in the acid parts, common minerals may have different compositions, and Sr isotope initial ratios are different. These net-veined parts can only be explained by the model of multiple injections whereby a felsic melt intruded into a basic magma.

Introduction

Intimate associations of acid and basic plutonic rocks have been reported from numerous intrusive complexes (e.g. Blake 1966; Walker and Skelhorn 1966; Yoder 1973; Wiebe 1973, 1974, 1979, 1980; Vogel and Wilband 1978; Eby 1979; Taylor et al. 1980; Bender et al. 1982; Wiebe and Wild 1983). On account of structural and textural relationships many of these occurrences have been attributed to coexisting acid and basic magmas. This raises the problem of explaining the origin of coexisting magmas of widely different compositions. In a number of cases there is convincing evidence that multiple injections of contrasted magmas took place and that the miscible magmas failed to mix completely due to high viscosities and rapid solidification (Wiebe 1974, 1980; Otto 1974; Taylor et al. 1980; Reid et al. 1983; Wiebe and Wild 1983). Such a process has been termed commingling. On the other hand, Bender et al. (1982) claimed that liquid immiscibility is a viable model for the origin of associated granodiorite and iron-rich diorite in the Rosetown-Cortlandt complex, N.Y., and similar models were proposed for parts of the alkaline province of the Monteregian Hills in Quebec (Philpotts and Hodgson 1968; Philpotts 1972, 1976; Eby 1979) and for parts of an anorthositic pluton in the Nain complex, Labrador (Wiebe 1979).

In order to evaluate the significance of the different mechanisms mentioned above, more detailed investigations of acid/basic plutonic associations including trace element and isotope studies are needed. In this paper, we present geological, petrographical, mineralogical, geochemical, and isotopic data on the various rock types of a small composite intrusive complex on the island of Samos, Greece, which exhibits structural features suggestive of both multiple injections of contrasted magmas and unmixing due to liquid immiscibility.

Offprint requests to: R. Altherr

Geological setting and field relations

The geological mapping of the island of Samos by Theodoropoulos (1979) revealed a small intrusive complex at Kallithea which hitherto has not been mentioned in the literature on Samos (Butz 1912; Philipson 1959; Papanikolaou 1979). K–Ar dating performed by H. Kreuzer on one hornblende concentrate (containing minor biotite) from a microdiorite gave a model age of 10.19 ± 0.15 Ma (0.223 ± 0.004 Nnl/g atmospheric Ar, 0.345 ± 0.004 Nnl/g radiogenic Ar, 0.8683 ± 0.0080 wt.% K) proving that the Kallithea complex belongs to the numerous Miocene granitoid intrusions of the Attic-Cycladic crystalline complex (Fig. 1; Altherr 1981; Altherr et al. 1982).

The Kallithea intrusive complex, which is situated at the western tip of the island of Samos (Fig. 2), is formed by numerous dikes measuring up to 30 m in width. It is well exposed over a length of about 2 km along a coastal cliff extending up to about 50 m above sea level. The complex can be completely viewed from the sea, but is not well accessible from land. Thus, the present investigations

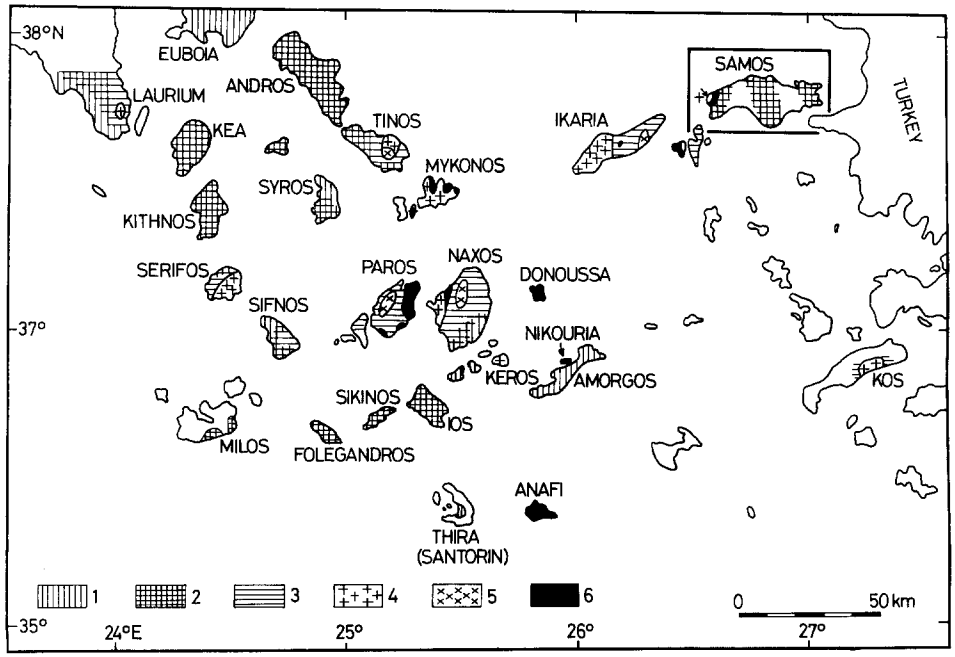

Fig. 1. Types of metamorphism and of granitoid rocks in the Attic-Cycladic crystalline complex. Lower unit (1–5): 1 = Eocene high P/T metamorphites, 2 = high P/T metamorphites considerably affected by low to medium P/T metamorphism during Oligocene/Miocene times, 3 = low to medium P/T metamorphites of Late Oligocene/Early Miocene age, 4 = I-type granitoids (Miocene), 5 = S-type granitoids (Miocene), 6 = upper unit undifferentiated

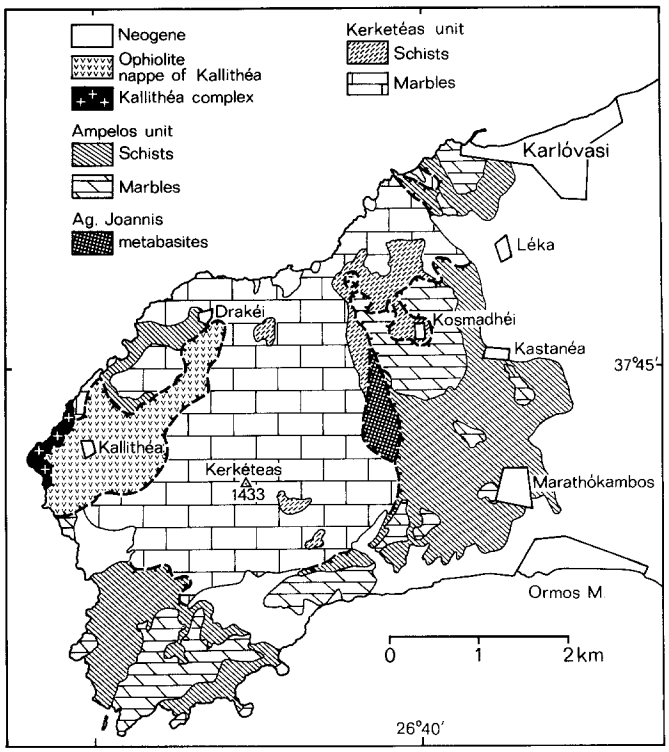

Fig. 2. Geological sketch map of western Samos

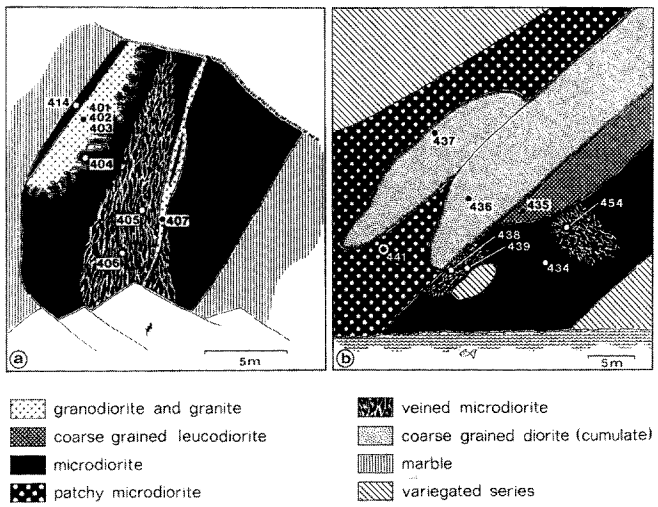

Fig. 3. Sketch of two representative composite dikes

are restricted to limited sections. The Kallithea igneous complex together with its country rocks is overthrust by a composite nappe consisting of Upper Triassic to Jurassic limestones and parts of an ophiolite sequence (Theodoropoulos 1979; Papanikolaou 1979). In the northern part of the complex, the country rocks of the intrusives are dolomitic marbles which contain rare silicate lenses or layers. To the south, the marbles are followed by a variegated sequence of calc-silicate rocks and amphibolites with minor intercalations of marbles and quartzites (Mezger and Okrusch 1985). In the marbles, most of the dikes are aligned subparallel to each other. They strike 160° and dip between 70° SW to 70° NE. The contacts to the marbles are always sharp and straight; apophyses are rare. In the variegated sequence, the subparallel alignment of the dikes is less well developed. Contacts tend to be more irregular and apophyses are frequent.

Whereas the thinner dikes only consist of microdiorite (for convenience we will group under this term all the fine to medium grained diorites and monzodiorites) or pyroxene leucodiorite, the thicker dikes are composite and contain two or more of the following rock types: pyroxene leucodiorite, coarse grained diorite, microdiorite, (quartz) monzonite, granodiorite to granite, and pegmatite. Structural relationships between these different rock types are manifold but nevertheless exhibit some kind of regularity (compare Fig. 3). Most of the dikes show a banded structure of microdiorites and granodiorites to granites; the latter

tend to be concentrated in the upper parts of the dikes. Contact relationships suggest that the granitic zones are younger than the microdioritic zones. Within the inhomogeneous granitic zones, transitions between parts of different compositions may be gradual or more gradational.

In the central parts of thicker microdiorite dikes, diffuse schlieren of coarse grained leucodiorite may be present. In the largest dike, which is exposed at the westernmost point of Samos, large xenoliths of coarse grained diorite are incorporated within microdiorite (Fig. 3b). In all dikes, younger dikelets of granodiorite, granite, pyroxene leucodiorite, as well as of pegmatites may cut older structures.

The microdioritic zones of some of the dikes contain spectacular net-veined parts in which spherical (pillow-like) to angular bodies of microdiorite are surrounded by a network of felsic rocks whereby the felsic veinlets make up between 10 and 20 vol.% of the whole net-veined parts. Contacts between microdiorite and felsic veinlets are always sharp. If the mafic pillows are flattened, they are orientated subparallel to the dikes (flow-deformation?). An age relationship between mafic pillows and felsic network cannot be established. Such structures may have originated by the intrusion of an acid melt into a basic magma. However, in none of the cases a connection of the felsic network to a filling pipe was observed. Hence, an origin of the net-veined parts by unmixing due to liquid immiscibility can be envisaged as well.

Analytical techniques

Microprobe analyses were carried out at the Max-Planck-Institut für Chemie at Mainz using an ARL microprobe equipped with a KEVEX energy dispersive system (acceleration potential 15 kV; sample current 5–6 nA; counting time 100 s) and at the Mineralogisches Institut der Universität Würzburg using a CAMECA M.S. 46 equipped with four wavelength dispersive spectrometers (quartz, PET, RbAP); acceleration potential 15 kV; sample current 300 nA; counting time 3×10 s; natural minerals, glasses, and pure metals were used for standardization.

Major elements and the trace elements Cr, Co, Ni, Cu, Zn, Rb, Sr, Pb, Th, Zr, Nb, and Y were determined by standard WDXRF techniques using lithium borate fusion disks and powder press tablets respectively. Standardization was done with international reference samples. Ba and, for those samples not studied by INAA, also La and Ce were measured by EDXRF using a radionuclide source (^{241}Am) for excitation and a planar Si(Li) detector (KEVEX) with 165 eV FWHD at 5.9 keV combined with a multichannel analyzer (4,096 channels). Detection limits were 5 ppm for Ba and 10 ppm for La and Ce. For standardization, international reference samples were used.

11 samples were analyzed by INAA for REE, Cr, Co, Ni, Sc, Ta, Cs, Th, U, and Hf. For standardization, primary solution standards were used. A set of three elements with no mutual interference of energies was combined to have multi-element standards. The international standard GSP-1 was run as a sample. Sample and standard capsules were irradiated simultaneously in the reactor TRIGA II at the Krebsforschungszentrum Heidelberg (DKFZ) under a thermal neutron flux of 8×10^{12} n cm^{-2} sec^{-1} for 5 h. Two detector systems were used for measuring the gamma spectra: an anticompton spectrometer equipped with a $9 \times 12''$ NaJ(Tl) guard detector and a HpGe central detector with 1.85 keV FWHD at 1.332 MeV (^{60}Co) covering the energy range from 150–2,000 keV and a high purity germanium detector for the energy range from 30–210 keV.

Fe^{2+} was analysed colorimetrically using a modified method of Ayranci (1977) as well as oxidimetrically (Peters 1968). H_2O was determined by Karl Fischer titration after thermal decomposition of the samples and by the Penfield method. CO_2 was analysed by IR gas absorption spectrometry after inductive heating and combustion of the sample in an atmosphere of oxygen (CSA 302, Leybold-Heraeus). Steal standards were used for calibration.

Rb–Sr isotope analyses were carried out at the Zentrallabor für Geochronologie (ZLG), University of Münster. Sample splits of about 100 mg were dissolved in Teflon beakers with $HF + HNO_3$ (3:1). For determinations of Sr concentrations, mixed ^{87}Rb–^{84}Sr spikes were used. Sr was separated by ion exchange techniques and was mounted with phosphoric acid on a single Ta filament. Blank determinations consistently yielded total Sr contents of less than 1 ng. Rb was measured by WDXRF. All errors are given at the 95% confidence level and correspond to twice the standard deviation of the mean value unless otherwise stated. Replicate analyses on splits of WR sample powders indicate a reproducibility within 0.01% of the ^{87}Sr/^{86}Sr ratios. Replicate measurements of NBS SRM 987 Sr-standard yielded a mean value of 0.71035 ± 4.

For details of the K–Ar dating see Altherr et al. (1982).

Petrography

Microdiorites

Microdiorite is the most abundant rock type in the dikes. The rocks consist of plagioclase, biotite, hornblende, K-feldspar, and quartz in variable proportions. Sphene, apatite, zircon, magnetite, and allanite are accessory phases. Relict clinopyroxene surrounded by hornblende and biotite was only found in one specimen. According to the IUGS nomenclature (Streckeisen 1976) the rocks can be classified as diorites and monzodiorites (Fig. 4; modal analyses are available on request). The texture is hypidiomorphic-granular, sometimes subophitic to ophitic. Hornblende may be concentrated in aggregates. In some parts of the dikes, the microdiorites contain patches which consist of plagioclase and minor K-feldspar surrounding hypidiomorphic to xenomorphic, often poikilitic grains of sphene. This type of rock will be referred to as patchy microdiorite.

The green hornblende shows a patchy color distribution and is strongly pleochroic. In some microdiorites the hornblendes have pale, weakly pleochroic cores showing irregular and gradual

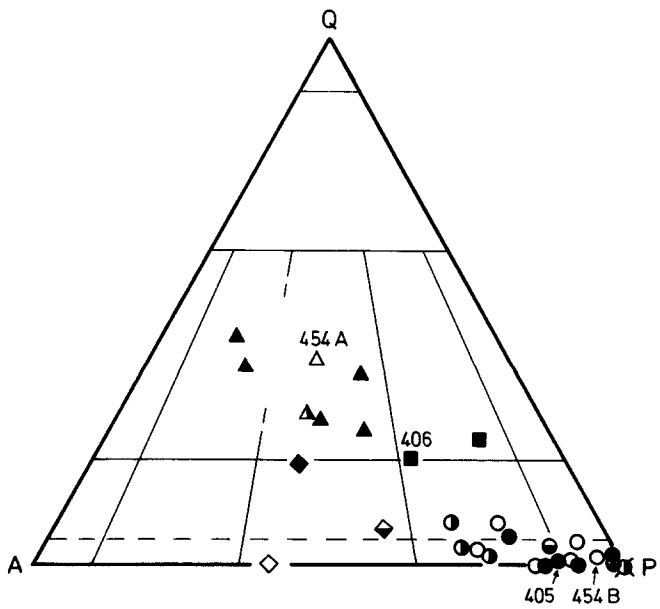

Fig. 4. Modal compositions of different rock types from composite dikes at Kallithea plotted in the diagram of Streckeisen (1976). *Triangles* = granites, *squares* = granodiorites, *diamonds* = monzonites, *circles* = microdiorites, *circles with diagonal crosses* = pyroxene leucodiorites, *circles with upright crosses* = coarse grained diorites (cumulates). Different fillings of symbols indicate different dikes

Table 1. Selected microprobe analyses of amphiboles

Rock type	Microdiorites								
Specimen	404				428			434	
Position in grain	Relict pale cores		Green core	Rim	Relict pale core	Transitional zone	Rim	Core	Rim
SiO_2	55.3	51.4	44.0	40.6	54.2	47.8	41.5	44.3	42.4
TiO_2	0.05	<0.05	0.87	1.41	<0.05	0.19	1.48	0.88	0.76
Al_2O_3	0.62	3.19	8.84	11.0	0.30	5.55	9.08	7.98	9.46
Fe_2O_3	1.4	1.6	6.0	6.5	1.6	5.7	6.7	6.8	7.0
FeO	11.5	13.3	12.7	13.7	13.2	12.0	14.1	14.3	14.7
MnO	0.21	0.23	0.29	0.24	0.71	0.46	0.58	0.47	0.48
MgO	15.8	14.3	10.8	9.17	14.7	12.3	9.22	9.31	8.66
CaO	13.3	12.5	11.9	11.6	12.6	11.9	11.7	11.9	11.6
Na_2O	<0.05	0.50	1.17	1.69	0.20	1.13	1.61	0.97	1.44
K_2O	<0.05	0.16	0.99	1.42	0.07	0.48	1.36	0.93	1.09
Total	98.18	97.18	97.56	97.33	98.08	97.51	97.33	97.84	97.59
Number of cations on the basis of 23 oxygens									
Si	7.903	7.537	6.606	6.209	7.889	7.091	6.371	6.693	6.471
Al^{IV}	0.097	0.463	1.394	1.791	0.051	0.909	1.629	1.307	1.529
Z	8.000	8.000	8.000	8.000	7.940	8.000	8.000	8.000	8.000
Al^{VI}	0.007	0.088	0.170	0.192	–	0.061	0.014	0.114	0.173
Fe^{3+}	0.151	0.177	0.678	0.748	0.175	0.636	0.774	0.773	0.804
Ti	0.005	–	0.098	0.162	–	0.021	0.171	0.100	0.087
Mg	3.365	3.125	2.417	2.090	3.189	2.720	2.110	2.097	1.970
Fe^{2+}	1.374	1.610	1.595	1.752	1.607	1.489	1.810	1.807	1.876
Mn	0.025	–	0.037	0.031	0.029	0.058	0.075	0.060	0.062
C	4.927	5.000	4.995	4.975	5.000	4.985	4.954	4.951	4.972
Mn	–	0.029	–	–	0.059	–	–	–	–
Fe^{2+}	–	0.021	–	–	–	–	–	–	–
Ca	2.036	1.964	1.914	1.901	1.965	1.891	1.924	1.926	1.897
Na	–	–	0.086	0.099	–	0.109	0.076	0.074	0.103
B	2.036	2.014	2.000	2.000	2.024	2.000	2.000	2.000	2.000
Na	–	0.142	0.255	0.402	0.056	0.216	0.403	0.210	0.323
K	–	0.030	0.190	0.277	0.013	0.091	0.266	0.179	0.212
A	–	0.172	0.445	0.679	0.069	0.307	0.669	0.389	0.535

boundaries against the green margins. Biotites are often intergrown with hornblende. Plagioclase contains inclusions of all the other minerals. Most of the grains are distinctly zoned with decreasing An contents from core to rim. Oscillatory zoning or patchy compositional differences occur in some of the An-rich cores. Sphene shows a distinct pleochroism. Many grains contain inclusions of optically anisotropic magnetite (confirmed by microprobe). Apatite occurs as fine needles which are often fractured. They frequently contain fluid inclusions. Allanite is xenomorphic or hypidiomorphic and displays a striking pleochroism with X (dark reddish brown 10 R 3/4) > Y (moderate brown 5 YR 5/%) > Z (olive 10 Y 6/2).

Granodiorites and granites

Besides K-feldspar, plagioclase, and quartz, these rocks consist of biotite, sphene, apatite, allanite, zircon, and magnetite (Fig. 4). Most of the rocks are medium grained; the rarer coarse grained granites are generally poorer in biotite.

Plagioclase is only weakly zoned. K-feldspar frequently shows a patchy extinction which sometimes grades into a well developed tartan twinning. Submicroscopic perthitic unmixing of albite is indicated by the presence of albite peaks in the powder diffraction patterns. Most of the biotite grains are at least partially replaced by rhipidolitic chlorite with exsolution of sagenite. Allanite is idiomorphic to hypidiomorphic and shows the same pleochroism as in the microdiorites. Some of the grains are discontinuously zoned. Apatite occurs in the form of stubby prisms and of more elongated columns.

Net-veined parts of the dikes

In all cases, the contacts between the mafic spherical (pillow-like) to angular bodies and the felsic rocks forming the network are sharp on both a megascopic and microscopic scale. The felsic vein-

Basic/acid pairs								Coarse grained diorite		Pyroxene leucodiorite	
Mdr 405		Gdr 406		Mdr 454B		MGr 454A		451		131	
Core	Rim	Core	Rim	Core	Rim	Core	Rim	Core	Rim	Core	Rim
43.9	42.8	44.0	42.7	44.0	43.2	43.9	43.0	53.4	48.2	53.9	53.3
0.76	0.63	0.84	0.91	0.90	0.91	1.23	0.83	0.13	0.93	0.08	0.08
8.94	9.89	8.79	9.52	8.80	9.02	8.73	9.58	2.71	7.1	2.79	2.69
6.2	6.5	6.2	6.5	6.1	6.3	6.0	6.4	1.2	1.3	1.1	1.2
13.1	13.6	13.1	13.7	12.7	13.2	12.5	13.4	9.3	10.9	8.8	9.7
0.38	0.44	0.51	0.47	0.52	0.50	0.48	0.50	0.23	0.23	0.12	0.27
10.5	9.82	10.3	9.91	10.5	10.2	10.4	9.81	17.1	14.5	18.1	16.8
11.8	11.8	11.9	11.6	11.9	11.9	11.7	11.6	12.7	12.4	11.8	12.7
1.23	1.11	1.29	1.43	1.32	1.38	1.50	1.49	0.30	0.93	0.23	0.32
0.93	1.10	0.95	1.13	0.96	1.05	1.03	1.09	0.18	0.58	0.16	0.13
97.74	97.69	97.88	97.87	97.70	97.66	97.47	97.70	97.25	97.07	97.08	97.19
6.595	6.469	6.608	6.457	6.608	6.526	6.605	6.497	7.647	7.048	7.676	7.652
1.405	1.531	1.392	1.543	1.392	1.474	1.395	1.503	0.353	0.952	0.324	0.348
8.000	8.000	8.000	8.000	8.000	8.000	8.000	8.000	8.000	8.000	8.000	8.000
0.178	0.231	0.164	0.154	0.166	0.132	0.153	0.203	0.104	0.272	0.144	0.107
0.701	0.739	0.701	0.740	0.689	0.716	0.679	0.728	0.129	0.143	0.118	0.130
0.086	0.072	0.095	0.103	0.102	0.103	0.139	0.094	0.014	0.102	0.009	0.009
2.351	2.212	2.306	2.234	2.350	2.297	2.322	2.209	3.650	3.160	3.842	3.595
1.646	1.719	1.645	1.733	1.595	1.688	1.573	1.693	1.103	1.323	0.887	1.159
0.038	0.027	0.065	0.036	0.066	0.064	0.061	0.064	–	–	–	–
5.000	5.000	4.976	5.000	4.968	4.980	4.937	4.991	5.000	5.000	5.000	5.000
0.010	0.029	–	0.024	–	–	–	–	0.028	0.028	0.014	0.033
–	–	–	–	–	–	–	–	0.011	0.010	0.161	0.006
1.900	1.911	1.915	1.879	1.915	1.926	1.886	1.878	1.949	1.943	1.801	1.953
0.090	0.060	0.085	0.097	0.085	0.074	0.114	0.122	0.012	0.019	0.024	0.008
2.000	2.000	2.000	2.000	2.000	2.000	2.000	2.000	2.000	2.000	2.000	2.000
0.268	0.265	0.291	0.322	0.289	0.330	0.324	0.314	0.071	0.245	0.040	0.081
0.178	0.212	0.182	0.218	0.184	0.202	0.198	0.210	0.033	0.108	0.029	0.024
0.446	0.477	0.473	0.540	0.483	0.532	0.522	0.524	0.104	0.353	0.069	0.105

lets range up to 5 cm in thickness. Whereas the mafic bodies consist of microdiorite having the same petrographical characteristics as the other homogenous microdiorites, the felsic veinlets do show important differences in their compositions. We investigated four representative pairs of associated microdiorite and felsic veinlets having the composition of monzonite (samples 439/438, Fig. 3b), quartz monzonite (426/427), granodiorite (405/406, Fig. 3a), and monzogranite (454 A/B, Fig. 3b). Mafic minerals of all the felsic veinlets are biotite and hornblende, as well as sphene, allanite, apatite, zircon, and magnetite. The microdiorite bodies do not show any difference in modal composition or grain size between their centers and their outer zones bordering on the felsic veinlets. Hence, their is no evidence that the basic magma was chilled against the acid one. In one of the four examples (sample 454 B), the microdiorite pillows contain ocelli up to several mm in diameter which resemble the monzogranitic veinlets (454 A) in texture and composition. The microdiorite 454 B differs from all the other microdiorites by having about 8 vol.% of magnetite.

Pyroxene leucodiorites

These rocks consist of hypidiomorphic to xenomorphic plagioclase and phenocrysts of diopsidic clinopyroxene partly replaced by fibrous actinolitic amphibole. Subordinate minerals are sphene, allanite, and apatite. Allanite has the same pleochroism as in the microdiorites, granodiorites, and granites.

Coarse grained diorites

These rocks which occur as isolated inclusions within the largest dike (Fig. 3b) display an orthocumulate texture. Idiomorphic to hypidiomorphic crystals of amphibole, up to 20 mm long and 8 mm broad, form the cumulus phase. The interstices are filled by aggregates or larger grains of xenomorphic plagioclase, accessory sphene, and rare clinopyroxene and pyrite. In most samples, the amphibole is heavily altered to chlorite and opaques. It has to

be pointed out that the coarse grained diorites are the only I-type rocks of the Kallithea complex which do not contain allanite.

Pegmatites

The pegmatites tend to have a higher ratio of K-feldspar over plagioclase than the granites. Areas particularly rich in K-feldspar show a poikilitic texture. Frequently, myrmekite is observed at the contacts between K-feldspar and plagioclase. In a few cases, garnet, muscovite, or magnetite are present as mafic minerals instead of biotite.

Mineral chemistry

Plagioclases

The An content of plagioclase ranges between 63 and 17 mol.% in the microdiorites and between 21 and 5 mol.% in the granodiorites and granites. Within the net-veined parts of the dikes the overall range of plagioclase compositions of all the felsic veinlets is An 33-21 which is similar to that of the associated microdiorites 439 (An 27-24) and 426 (An 32–24). The microdiorites 405 and 454 B, however, contain plagioclases with core compositions ranging up to 55 mol.% An.

Plagioclases in the coarse grained diorites are more calcic (An 55-23) than those in the pyroxene leucodiorites (An 33-22).

Amphiboles

Selected amphibole analyses are given in Table 1. Formulae of the green hornblendes were calculated assuming that FeO = 0.7 FeO_{tot} whereas for the pale amphiboles a lower oxidation ratio of FeO = 0.9 FeO_{tot} was used (see Altherr 1981 for a justification of these ratios).

The green hornblendes of the normal microdiorites show a continuous zoning with decreasing Si, Mg, and Na/K and increasing Al_{total}, Al^{IV}, Fe_{total}, Ti, Na, and K from core to rim (Fig. 5A). According to the I.M.A. nomenclature compiled by Leake (1978), these hornblendes range from magnesio-hornblendes in the cores to tschermakitic, edenitic, and magnesian hastingsitic hornblendes in the rims. The relict pale cores present in some microdiorites (404, 428) are actinolites to actinolitic hornblendes with higher Mg/Fe and Na/K than the surrounding green hornblendes (Fig. 5A).

The green hornblendes from the basic/acid pairs (microdiorite 405/granodiorite 406 and microdiorite 454 B/monzogranite 454 A) do not show a strong zoning. As can be seen from Fig. 5B, C the hornblendes of the basic and acid parts in both cases have the same compositions.

The compositions of the amphiboles from the coarse grained diorites (cumulates) range from actinolitic in the cores to actinolitic hornblendes in the rims (Table 1). These amphiboles are richer in Mg than the relict actinolites and actinolitic hornblendes of the microdiorites, but show the same range in composition as the amphiboles replacing clinopyroxene in the pyroxene leucodiorites.

Biotites

Selected biotite analyses are given Table 2. Formulae were calculated assuming that FeO = 0.87 FeO_{tot} (see Altherr 1981 for a justification of this ratio).

All biotites investigated are poor in Al, as can be expected for biotites from I-type granitoids. In the diagram of Nockolds (1947) they all plot into field III representing biotites of hornblende-bearing granitoids (Fig. 6). Using the nomenclature of Foster (1960), the biotites can be classified as transitional between Fe-biotites and Mg-biotites. Compositional inhomogeneities within the grains are small and irregularly distributed.

The biotites from the two basic/acid pairs 405/406 and 454 B/454 A do not show compositional differences and are richer in Mg but lower in Ti than the biotites of all the other rock types (Table 2 and Fig. 6).

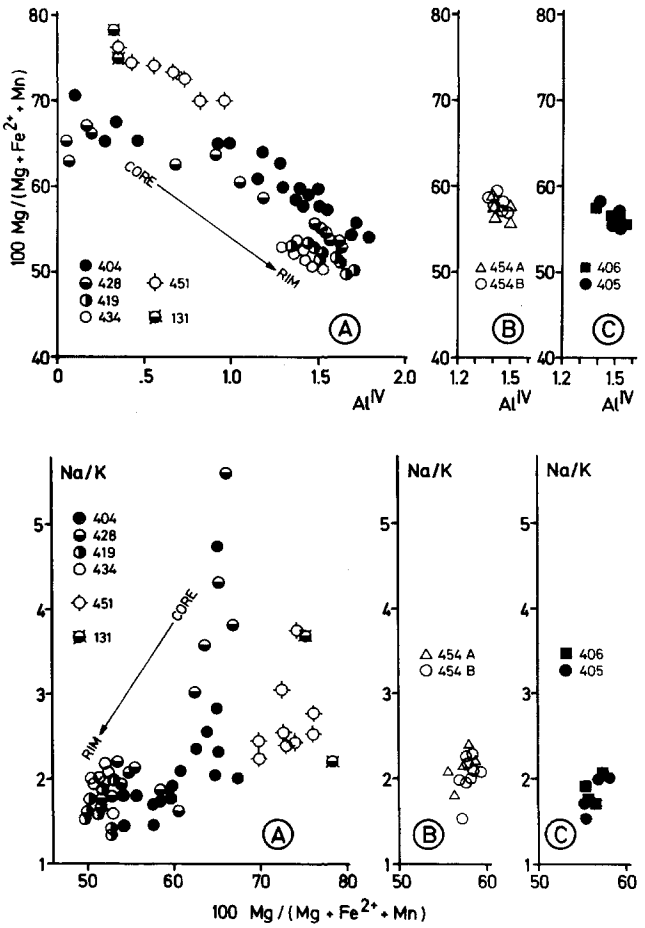

Fig. 5. Composition of amphiboles from different rock types. Upper part: Variation of 100 Mg/(Mg + Fe^{2+} + Mn) with Al^{IV}. Lower part: Variation of Na/K with 100 Mg/(Mg + Fe^{2+} + Mn). Symbols as in Fig. 4. For further explanation see text

Clinopyroxenes

The clinopyroxenes of the pyroxene leucodiorites show significantly higher Mg/(Mg + Fe) than the amphiboles replacing them (Tables 1 and 3).

Sphenes

Sphenes of all rocks contain substantial amounts of Fe and Al substituting for Ti. Larger grains are often inhomogeneous with the tendency of increasing Al and Fe from core to rim. Sphenes of the granites have relatively higher contents of Al compared with those of the microdiorites (Fig. 7A). In Fig. 7B sphenes from the basic and acid parts of veined diorites are plotted. The sphenes from the basic parts plot within the field of sphenes from the other microdiorites. Whereas the sphenes from the acid part 406 plot within the field of sphenes from granites, i.e., are rich in Al, the sphenes from the acid part 454 A have the same composition as those from the basic part 454 B, i.e., are richer in Fe^{3+} (Fig. 7B).

Discussion of mineral compositions

If two immiscible liquids crystallize in continuous equilibration with one another, minerals common to both will have

Table 2. Microprobe analyses of biotites (mean values)

Rock type	Microdiorites				Granite	Basic/acid pairs			
Specimen	404	419	428	434	124	Mdr 405	Gdr 406	Mdr 454B	MGr 454A
SiO_2	36.5	36.1	36.0	35.8	35.7	36.9	37.0	36.9	36.5
TiO_2	3.31	3.75	3.28	3.46	4.07	2.97	2.95	2.85	2.99
Al_2O_3	14.4	14.6	14.9	14.7	14.5	14.8	14.8	14.6	14.5
Fe_2O_3	3.0	3.2	3.0	3.3	3.5	2.8	2.8	2.8	3.0
FeO	18.1	19.0	18.2	19.9	20.9	16.9	17.0	16.8	17.9
MnO	0.23	0.19	0.15	0.18	0.18	0.21	0.16	0.24	0.23
MgO	11.3	10.2	10.9	9.42	8.17	12.3	12.2	12.3	11.6
CaO	0.08	0.09	0.09	0.10	0.12	0.11	0.11	0.08	0.12
Na_2O	0.11	0.09	0.19	0.09	0.14	0.10	0.14	0.11	0.10
K_2O	9.49	9.35	9.48	9.30	9.21	9.59	9.30	9.50	9.24
Total	96.52	96.57	96.19	96.25	96.49	96.68	96.46	96.18	96.18
Number of cations on the basis of 11 oxygens									
Si	2.764	2.745	2.739	2.745	2.745	2.769	2.778	2.782	2.767
Al^{IV}	1.236	1.255	1.261	1.255	1.255	1.231	1.222	1.218	1.233
Z	4.000	4.000	4.000	4.000	4.000	4.000	4.000	4.000	4.000
Al^{VI}	0.049	0.053	0.075	0.073	0.059	0.078	0.088	0.079	0.063
Fe^{3+}	0.171	0.183	0.172	0.190	0.203	0.158	0.158	0.159	0.171
Ti	0.189	0.214	0.188	0.199	0.235	0.168	0.167	0.162	0.170
Mg	1.276	1.156	1.236	1.076	0.936	1.376	1.366	1.382	1.311
Fe^{2+}	1.146	1.208	1.158	1.276	1.344	1.061	1.068	1.059	1.135
Mn	0.015	0.012	0.010	0.012	0.012	0.031	0.010	0.015	0.015
Y	2.846	2.826	2.839	2.826	2.789	2.854	2.857	2.856	2.856
Ca	0.006	0.007	0.007	0.008	0.010	0.009	0.009	0.006	0.010
Na	0.016	0.013	0.028	0.013	0.021	0.015	0.020	0.016	0.015
K	0.917	0.907	0.920	0.910	0.903	0.918	0.891	0.914	0.894
X	0.939	0.927	0.955	0.931	0.934	0.942	0.920	0.936	0.919

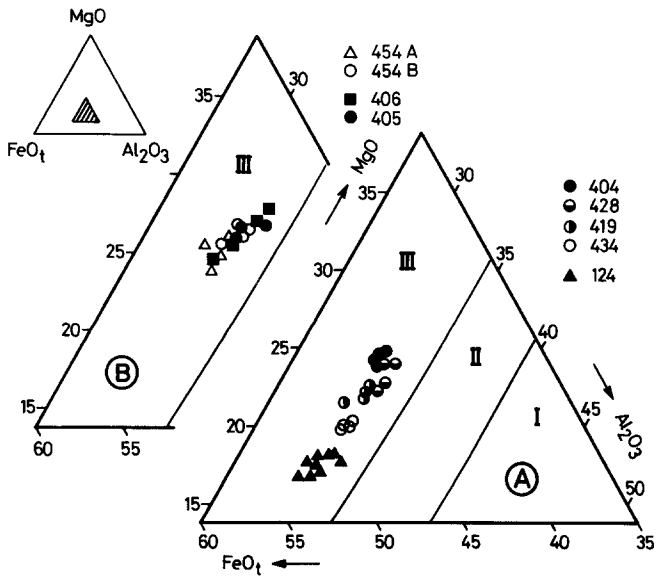

Fig. 6. Composition of biotites from different rock types plotted in the diagram of Nockolds (1947). I = field of biotites coexisting with muscovite (S-type granitoids), II = field of biotites from S-type granitoids without muscovite, III = field of biotites from I-type granitoids with hornblende. Components are plotted as wt.% ratios. Symbols as in Fig. 4

the same compositions (Bowen 1928). Suppose, the acid-basic rock pairs in the net-veined parts of the Kallithea dikes represent former immiscible liquids, and equilibrium was maintained during crystallization, then plagioclases, hornblendes, biotites, and sphenes in each pair should have identical compositions. In the case of the two pairs investigated (405/406 and 454 B/454 A), this holds true for the hornblendes and biotites (Figs. 5 and 6), and also for the plagioclases if we disregard the An-rich cores in the basic parts. Sphene compositions, however, are similar only for the pair 454 B/454 A, but differ for the pair 405/406 (Fig. 7). However, the test of identical mineral compositions is not strictly applicable because continuous equilibration cannot be expected to occur in all natural systems. The An-rich cores in the two microdioritic parts 405 and 454 B could be explained by the following model: The first plagioclase crystals formed in both conjugate melts had the same An-rich compositions but in the acid magma where little of this mineral was formed, solid diffusion with later layers eliminated the early cores, whereas in the basic magma the larger crystals of this An-rich compositions persisted as cores. So far, we have no conclusive model to explain the different sphene compositions of the pair 405/406 (Fig. 7). Mineral compositions could be different, if the two liquids solidified in closed systems after the process of unmixing.

Table 3. Selected microprobe analyses of clinopyroxene from pyroxene leucodiorite 131

	Core	Rim
SiO_2	53.4	53.9
Al_2O_3	0.40	0.12
FeO	5.88	4.85
MnO	0.10	0.15
MgO	14.8	15.4
CaO	25.0	25.2
Na_2O	0.37	0.20
Total	99.95	99.82
Number of cations on the basis of 6 oxygens		
Si	1.981	1.992
Al^{IV}	0.017	0.005
Z	1.998	1.997
Fe^{2+}	0.182	0.150
Mn	0.003	0.005
Mg	0.818	0.848
	1.003	1.003
Ca	0.994	0.998
Na	0.024	0.014
	1.021	1.012

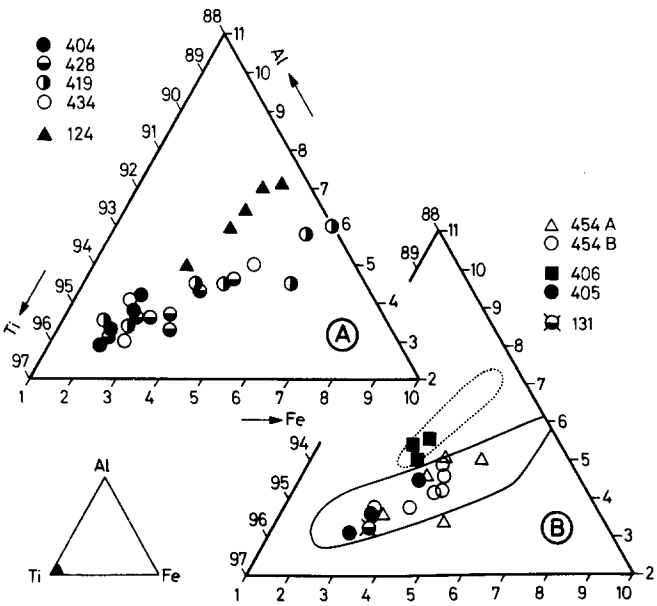

Fig. 7. Composition of sphenes from different rock types (atomic proportions of Ti, Al, and Fe). Symbols as in Fig. 4

We conclude, that, on the basis of mineral compositions, the pair 454 B/454 A may well represent two immiscible liquids which essentially crystallized in continuous equilibration with one another, but such a model does not necessarily hold true for the pair 405/406.

Bulk rock chemistry

Selected bulk rock analyses of all the different I-type rocks are given in Tables 4 and 5. The pegmatites were not analysed because of their strong secondary alteration. We will start our discussion with those rocks for which an origin by unmixing due to liquid immiscibility can be excluded at the level of outcrop and then we will turn to the net-veined parts of the dikes.

Pyroxene leucodiorites and coarse grained diorites

In Harker diagrams (Fig. 9) these rocks form distinct groups and plot off the indistinct trends defined by the microdiorites, granodiorites, and granites. Chemical characteristics of the *pyroxene leucodiorites* are relatively high contents of Ca, Y, Na, Zn, Nb, and Th, and relatively low contents of Ti, P, K, Rb, Pb, Ba, and Sr. Therefore, these rocks are regarded to represent an independent pulse of magma, presumably not related to the other rocks. The *coarse grained diorites* interpreted as cumulates on petrographical grounds have relatively low contents of Na, Al, Ti, P, Nb, Zr, Th, LREE, K, Rb, Pb, Ba, and Sr, but high contents of Ca, Mg, Cr, and Ni (Tables 4 and 5, Fig. 9). Hence, these rocks show a typical cumulate chemistry. We are, however, not able to decide whether these rocks represent early segregates of a magma later forming the microdiorites or, alternatively, are genetically unrelated to the other rocks.

Microdiorites, granodiorites, and granites

All these rocks together form indistinct trends in chemical variation diagrams, a feature common to many I-type granitoid complexes (e.g., Altherr 1981; Fourcade and Allègre 1981; Reid et al. 1983). Consequently, the relationship between these different rocks cannot solely be explained by such simple mechanisms as fractional crystallization, two-component magma mixing or unmixing, or different degrees of partial melting of the same source. This is corroborated by the contents of REE. In Fig. 8E, the patterns of one microdiorite, one granodiorite, and one monzogranite sampled from one composite dike (Fig. 3A), are plotted. There is no systematic relationship between the relative positions of the patterns and the respective rock types. All rocks have similar contents in La, but the middle and heavy REE abundances are intermediate in the microdiorite, highest in the granodiorite, and lowest in the monzogranite.

Net-veined parts

The microdiorites from the net-veined parts have the same chemical compositions as the other microdiorites (Tables 4 and 5, Fig. 9). Whereas the felsic veinlet of granodioritic composition (406) cannot be distinguished from the other granodiorites (Tables 4 and 5, Fig. 9), the monzogranitic veinlet 454 A differs from all the other granodiorites to granites by having much lower contents of most HFS elements (e.g., P, middle and heavy REE, Zr, Hf, Nb, Ta; Tables 4 and 5, Figs. 8 and 9). The monzonitic and quartz monzonitic veinlets are characterized by remarkably high contents of Ba and Zr.

Fields of liquid immiscibility have been mapped out experimentally in simple quarternary model systems (see

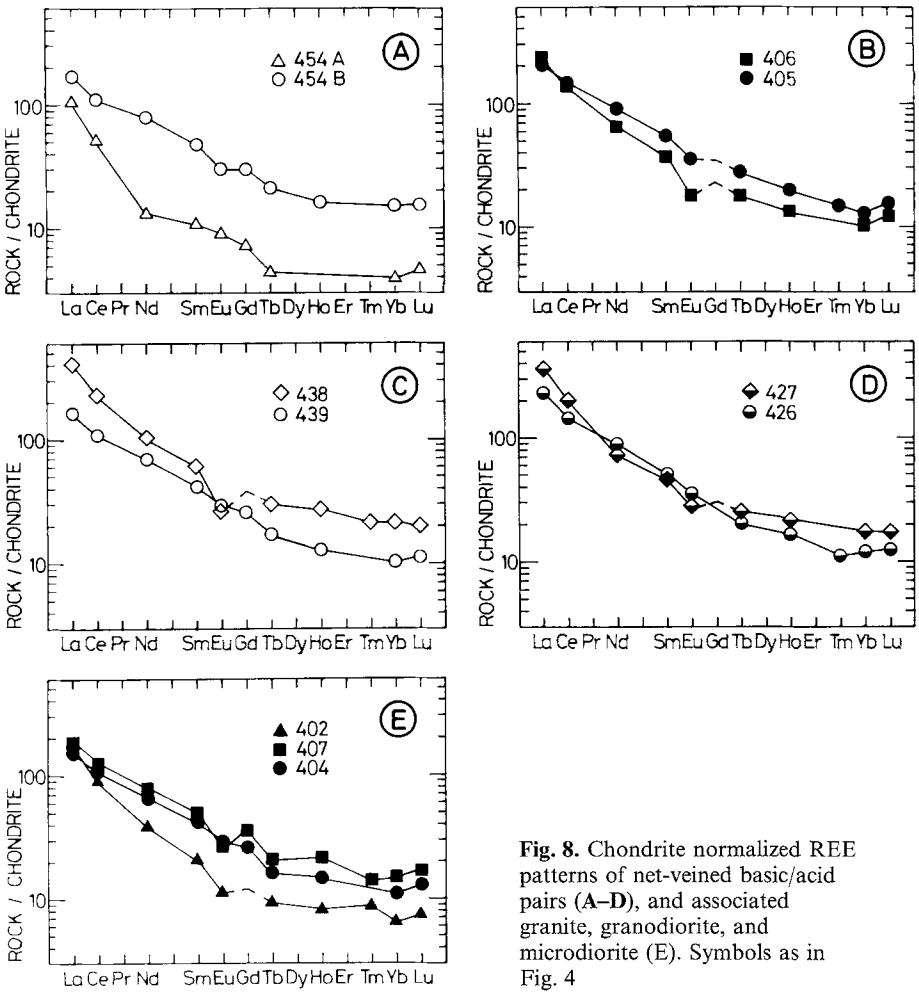

Fig. 8. Chondrite normalized REE patterns of net-veined basic/acid pairs (**A–D**), and associated granite, granodiorite, and microdiorite (E). Symbols as in Fig. 4

Roedder 1979 for discussion). It has been shown that liquid immiscibility is greatly influenced by parameters such as Na/K, Al, oxygen fugacity, water pressure, etc. For multicomponent natural rock systems, especially for those rich in alkalies and alumina, there are not enough data to use bulk rock compositions as a reliable criterion for or against liquid immiscibility. Furtheron, positions of rock compositions on pseudoternary plots (e.g., a Greig plot) in itself do not provide conclusive evidence. Nevertheless, the four investigated pairs have been plotted in a Greig diagram (Fig. 10). For comparison, Fig. 10 also contains the tielines for various conjugate volcanic rocks for which an origin by liquid immiscibility has been suggested (Roedder 1979; Fig. 2–8C) although the compositions of these rocks are not coincident with the edge of the known immiscibility field in the system leucite-fayalite-SiO_2 projected into the Greig diagram.

Because we deal with holocrystalline rocks there are further problems reducing the applicability of major element compositions (Greig plots) as criterion for liquid immiscibility: (1) A liquid can unmix by simple cooling or by cooling and crystallization. We therefore do not know whether the bulk rock compositions represent immiscible liquids or mixtures of such liquids with common crystals which were already present at the time of unmixing. The amounts of such crystals present in each liquid phase after unmixing may be very different and will be governed by such factors as viscosities of the two melts, sizes of globules and crystals, and preferential wetting of crystals. This may result in different positions and crossing tielines in the Greig diagram even for thermodynamically identical bulk systems; (2) After globules of a second melt have formed and cooling proceeds at equilibrium, each of the two melts as well as existing solid solutions will change their compositions by diffusion within the phases and across the interfaces. However, diffusion rates within the two liquids may differ greatly and, as a consequence, equilibrium might not be maintained. At a certain point in the cooling history, the two liquids might start to crystallize as closed systems. All these possibilities can result in different positions of the resulting rocks in the Greig diagram, although the systems were identical shortly after unmixing.

Although the distribution of major elements between coexisting immiscible magmas may yield compositions resembling those from crystal fractionation or from different degrees of partial melting, there are important differences in the partitioning of minor elements. From theoretical considerations as well as experimental evidence, we know that in the case of liquid immiscibility, the HFS elements are strongly partitioned into the basic melt whereas the LIL elements are enriched in the acid liquid (Ryerson and Hess 1978; Watson 1976). The elemental ratios between basic

Table 4. Selected bulk rock analyses

Rock type	Microdiorites				Granodiorites and Granites			
Specimen	404	419	428	434	124	402	403	407
SiO_2	51.5	53.3	49.4	52.6	65.9	70.7	73.0	61.4
TiO_2	1.41	1.34	1.75	1.43	0.61	0.39	0.19	1.04
Al_2O_3	17.7	18.4	18.2	18.3	16.0	14.7	14.4	16.2
Fe_2O_3	2.10	3.16	2.93	1.61	1.00	0.74	0.00	1.53
FeO	6.17	5.37	7.30	6.53	2.44	1.55	0.55	2.67
MnO	0.12	0.15	0.17	0.15	0.06	0.05	0.02	0.05
MgO	4.74	2.92	4.01	3.18	1.05	0.69	0.36	1.85
CaO	7.83	5.67	6.81	6.00	2.59	1.94	1.65	5.25
Na_2O	4.38	4.56	4.29	4.32	3.68	3.74	3.36	4.83
K_2O	1.82	3.50	2.68	3.44	4.67	4.68	5.40	2.44
P_2O_5	0.42	0.69	0.51	0.70	0.30	0.12	0.08	0.40
H_2O	1.31	1.14	1.67	1.63	0.9	0.38	0.25	0.72
CO_2	–	–	–	–	0.05	–	–	1.28
Total	99.50	100.20	99.72	99.89	99.25	99.68	99.26	99.66
Cr	7.8	14	14	14	–	8.0	5	6.8
Co	26	28	38	31	–	1.6	1	11.2
Ni	14	7	7	4	8	2.8	5	4.5
Sc	20	–	–	–	–	1.9	–	10
Cu	19	18	25	23	14	4	2	6
Zn	77	81	94	98	50	19	15	34
Rb	62	113	101	104	128	93	174	105
Sr	721	683	698	716	428	426	314	393
Ba	628	1,420	922	1,500	1,250	1,610	1,260	736
Ta	0.96	–	–	–	–	0.83	–	1.37
Cs	2.5	–	–	–	–	1.7	–	3.5
Pb	15	20	15	26	31	31	45	19
Th	8.9	11	13	13	52	25	15	19
U	3.1	–	–	–	–	5.3	–	6.1
Zr	178	127	151	243	347	182	123	251
Hf	4.33	–	–	–	–	5.09	–	6.66
Nb	19	21	21	19	17	12	13	24
Y	27	31	35	35	25	16	17	34
La	–	52	54	74	135	–	28	–
Ce	–	101	108	133	186	–	44	–

Mdr = Microdiorite, Gdr = Granodiorite, Mz = Monzonite, QMz = Quartz monzonite, MGr = Monzogranite

and acid parts of the four rock pairs investigated are presented in Table 6. It can be seen that only the pair microdiorite 454 B/monzogranite 454 A essentially fulfils these requirements. For this pair, the ratios for the middle and heavy REE, Zr, P, and Ti compare well with the experimental values of Watson (1976) and Ryerson and Hess (1978), but are much lower (sometimes even <1) for the other pairs. These relationships are also visualized in the REE patterns (Fig. 8). Except for the LREE, the pair 454 B/A (Fig. 8A) shows almost parallel patterns with much lower REE abundances of the acid part compared to the basic one. In contrast, the other three pairs exhibit much smaller differences in the REE contents between basic and acid parts. Pair 438/439 (Fig. 8C) even shows higher REE concentrations in the acid part 438; pair 426/427 (Fig. 8D) displays cross-cutting patterns.

Summarizing, we may state that liquid immiscibility is a possible model to explain the chemical compositions of pair 454 B/454 A, but not of the other pairs which have to be explained by multiple intrusions of magmas not related to each other by unmixing due to liquid immiscibility.

$^{87}Sr/^{86}Sr$ initial ratios

Rb-Sr isotopic data of the two basic/acid pairs 454 B/A and 405/406, as well as of granite 402 from the same dike (Fig. 3a, b) are presented in Table 7. Initial ratios were calculated for each sample by assuming an intrusion age of 12 Ma.

In a Nicolaysen diagram, the five samples do not at all define an isochron; a feature not uncommon to many composite I-type granitoid complexes (e.g., Altherr et al. 1982; Halliday et al. 1980). The differences in the initial ratios are not regarded to be due to secondary (hydrothermal) alteration, but are interpreted to reflect primary differences inherited from the source rocks which means the rocks are not comagmatic in the strict sense. Similar observations were made by Altherr et al. (1984) in other Miocene I-type complexes of the central Aegean.

Interestingly, the basic/acid pair 454 B/A shows nearly identical initial ratios, a further argument in favour of an origin by liquid immiscibility. Not unexpectedly, the other pair 405/406 exhibits significantly different initial ratios de-

Basic/acid pairs								Coarse grained diorite	Pyroxene leucodiorite
Mdr 405	Gdr 406	Mdr 426	QMz 427	Mdr 439	Mz 438	Mdr 454B	MGr 454A	451	131
51.8	65.5	48.9	57.1	52.0	59.3	53.2	71.9	53.5	57.4
1.60	0.57	1.32	0.77	1.15	0.68	1.80	0.30	0.92	0.25
17.7	14.7	19.0	18.6	15.7	18.6	17.3	13.6	12.1	17.9
2.58	0.99	3.14	2.21	2.32	2.38	4.15	0.88	0.77	0.21
6.15	3.02	6.20	3.35	6.13	1.65	5.66	0.89	7.55	1.13
0.13	0.04	0.13	0.06	0.17	0.06	0.16	0.02	0.20	0.06
4.05	1.97	3.76	1.66	6.23	1.46	3.56	0.56	10.2	3.44
6.73	2.72	6.49	3.49	9.27	2.86	5.77	2.01	9.30	9.64
4.02	3.91	4.39	4.48	3.76	4.20	4.94	3.70	2.31	6.18
3.10	3.12	2.55	4.98	1.91	6.87	1.96	3.41	1.08	0.40
0.49	0.21	0.86	0.40	0.36	0.29	0.48	0.09	0.19	0.07
1.15	1.66	2.05	1.46	1.36	1.07	1.11	0.62	2.19	0.47
–	1.22	1.03	0.98	–	0.08	–	0.14	–	2.11
99.50	99.63	99.82	99.54	100.36	99.50	100.09	98.12	100.31	99.26
7.8	7.2	6.3	9.3	112	9.3	4.8	2.7	278	4
23	9.0	23	6.5	39	9.1	24	3.6	34	3
7	7.0	6.9	5.8	37	6.1	6	4	169	3
18	8.5	10	5.7	26	6.4	17	1.3	–	–
18	5	18	9	12	32	24	6	9	1
80	43	97	55	99	41	104	26	104	36
97	61	81	112	44	154	85	64	26	8
620	490	882	672	637	709	475	459	305	390
990	1,350	1,420	2,570	860	2,820	450	1,370	298	153
1.00	1.93	0.90	1.33	0.74	2.42	1.14	0.67	–	–
4.0	0.5	2.2	0.92	0.39	1.6	3.6	0.75	–	–
25	18	21	25	14	39	21	26	6	12
16	25	14	27	14	36	13	50	4	23
4.6	5.6	3.5	6.2	4.2	6.0	4.3	11	–	–
237	241	235	426	121	343	223	152	117	124
5.64	6.50	5.70	10.5	3.31	10.2	5.15	4.30	–	–
22	27	20	18	15	32	23	7	15	49
33	25	31	31	29	47	37	11	31	26
–	–	–	–	–	–	–	–	30	–
–	–	–	–	–	–	–	–	55	–

Table 5. Rare earth element data (INAA)

Rock type	Micro-diorite	Granodiorites and Granites		Basic/acid pairs							
Specimen	404	402	407	Mdr 405	Gdr 406	Mdr 426	QMz 427	Mdr 439	Mz 438	Mdr 454B	MGr 454A
La	48.3	53.4	56.6	66.8	72.0	71.1	112	52.1	132	53.2	34.1
Ce	86.4	75.3	100	118	111	119	163	86.9	188	91.1	48.1
Nd	38.7	22.9	46.4	54.5	39.2	52.7	44.7	40.7	62.5	46.6	7.4
Sm	7.91	4.00	9.24	10.5	7.02	9.28	9.05	8.02	11.2	9.04	2.06
Eu	2.09	0.81	1.99	2.60	1.27	2.53	1.99	2.04	1.98	2.15	0.64
Gd	6.8	–	9.2	–	–	–	–	6.6	–	7.7	1.9
Tb	0.79	0.46	1.03	1.26	0.87	0.99	1.24	0.84	1.43	1.03	0.22
Ho	1.09	0.61	1.57	1.45	0.94	1.21	1.53	0.94	2.02	1.20	–
Tm	–	0.28	0.45	0.46	–	0.34	–	–	0.68	–	–
Yb	2.28	1.36	3.09	2.65	2.13	2.50	3.67	2.11	4.44	3.16	0.79
Lu	0.42	0.24	0.55	0.51	0.40	0.41	0.58	0.37	0.64	0.50	0.16

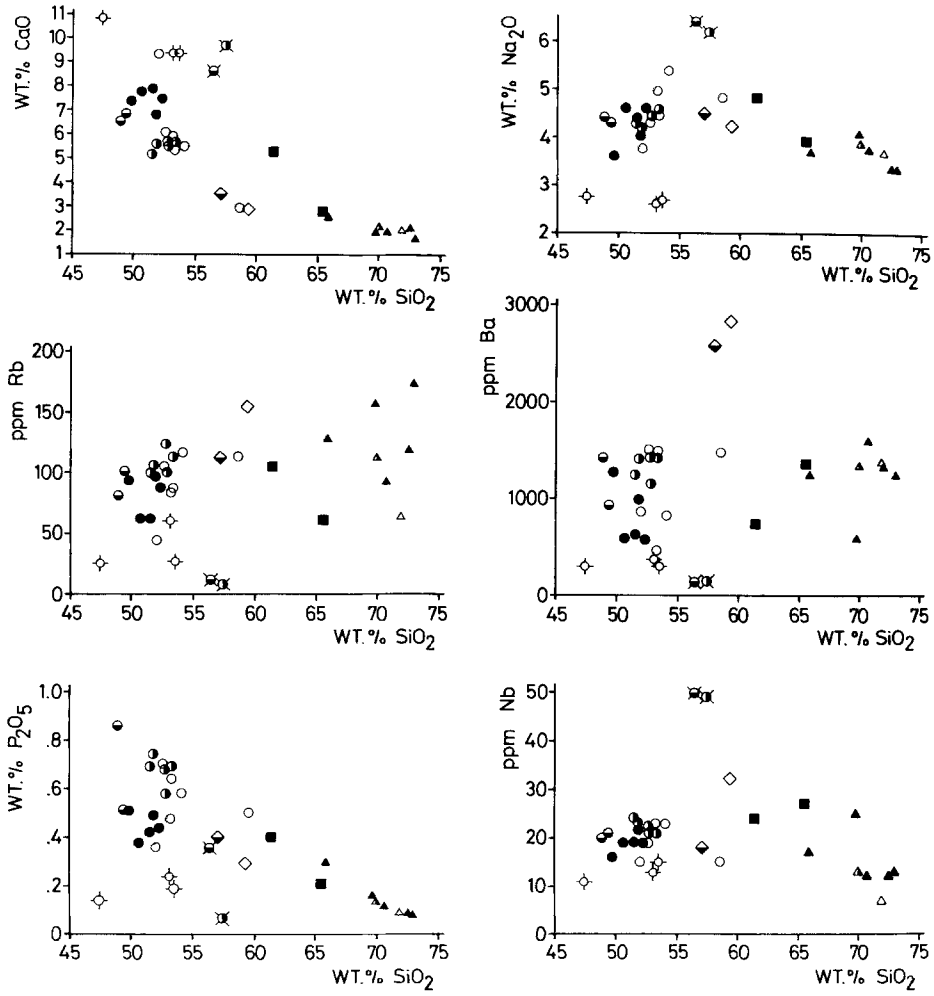

Fig. 9. Selected Harker diagrams for all investigated samples. Symbols as in Fig. 4

finitively ruling out a comagmatic relationship between the two parts of this net-veined microdiorite. The granite 402 coming from the same composite dike even has a much lower initial ratio. For the three rocks of this dike, no correlation exists between Rb/Sr and the Sr initial ratio, excluding a simple mixing model between a Rb-rich older crustal component and a Sr-rich mantle component.

Conclusions

Field relations clearly indicate that the composite dikes of the Kallithea complex were formed by multiple injections of compositionally different magmas. Like in many other composite granitoid complexes petrographical and geochemical data alone do not in all cases provide conclusive evidence for or against a comagmatic relationship between the different magma pulses. Sr isotope data, however, prove that at least some of the different magma pulses were genetically unrelated.

The predominant rock types in the Kallithea complex are various types of microdiorites, granodiorites, and granites. All these rocks show striking mineralogical similarities. They contain hornblendes, biotites, and sphenes of roughly similar compositions, and allanite with the same spectacular pleochroism. Furthermore these rocks form at least indistinct trends in chemical variation diagrams (Fig. 9) and reveal geochemical characteristics which are typical of orogenic monzonite series, i.e., high contents of Ba, Sr, Th, Pb, strong LREE enrichment, relatively low contents of Rb and low initial Sr isotope ratios. There are striking similarities with the monzonitic complexes of the island of Kos (Altherr 1981) and of the Bodrum peninsula, Turkey (Robert and Cantagrel 1977). Thus, the Kallithea intrusive complex fits well into the regional compositional pattern formed by all Miocene I-type intrusives of the central Aegean, interpreted by Altherr et al. (1982) and Seidel et al. (1982) as part of a classical paired belt (Fig. 1).

The most interesting problem is posed by the net-veined parts of the dikes in which small bodies of microdiorite are surrounded by a network of felsic rocks (Fig. 3). The structural and petrographical features are consistent with an origin by multiple injections and commingling of contrasted magmas, but could also be explained by unmixing due to liquid immiscibility. Mineralogical, geochemical, and Sr isotope data show that formation by unmixing due to liquid immiscibility has to be excluded for the pairs 439/438 (monzonite), 426/427 (quartz monzonite), and 405/406 (granodiorite). Only the pair 454 B/454 A (monzogranite) provides strong supporting evidence for an origin by unmixing due to liquid immiscibility: (a) The basic pillows contain ocelli of the same composition as the acid veinlets; (b) All the minerals common to both the basic and acid parts have the same compositions except for the An-rich cores of plagioclases in the basic part which can easily be explained by lacking reequilibration during the initial stages of crystyllization; (c) The HFS elements are strongly enriched in

Table 6. Partitioning data of basic/acid rocks

Element	454B/ 454A	405/406	426/427	439/438	A	B
K	0.57	0.99	0.51	0.28	0.45	0.21
Fe	5.58	2.16	1.69	2.18	2.18	4.02
Al	1.27	1.20	1.02	0.84	0.64	0.58
Si	0.74	0.79	0.86	0.88	0.75	0.61
Mn	8.0	3.25	2.17	2.83	2.93	5.0
Ba	0.33	0.73	0.55	0.30	1.50	~ 1
Sr	1.03	1.27	1.31	0.90	1.54	~ 1
Mg	6.35	2.06	2.27	4.27	2.15	6.0
Cr	1.78	1.08	0.68	12.0	3.76	–
Zr	1.47	0.98	0.55	0.28	2.36	–
Hf	1.20	0.87	0.54	0.32	–	–
P	5.33	2.33	2.15	1.24	10.8	24
Ti	6.00	2.81	1.71	1.69	3.08	3.90
Rb	1.33	1.07	0.72	0.29	–	~ 1
Ta	1.70	0.52	0.68	0.30	4.31	–
La	1.56	0.93	0.63	0.39	3.91	~10
Ce	1.89	1.06	0.73	0.46	–	–
Nd	6.30	1.39	1.18	0.65	–	–
Sm	4.39	1.50	1.03	0.72	4.42	~10
Eu	3.36	2.05	1.27	1.03	–	–
Gd	4.05	–	–	–	–	–
Tb	4.68	1.45	0.80	0.59	–	–
Yb	4.00	1.24	0.68	0.48	–	~10
Lu	3.13	1.28	0.71	0.58	4.18	–
Nb	3.29	0.81	1.11	0.47	–	–
Y	3.36	1.22	1.00	0.62	–	–

A = experimental data of Watson (1976)
B = experimental data of Ryerson and Hess (1978)

Table 7. Rb-Sr whole rock data

Sample	Rb (XRF) (ppm)	Sr (ppm)	$\frac{^{87}Rb}{^{86}Sr}$	$^{87}Sr/^{86}Sr$	$(^{87}Sr/^{86}Sr)$ t = 12 Ma
402	93	426.3	0.63	0.70640 ± 2	0.70629
405	97	619.7	0.44	0.70696 ± 6	0.70689
406	61	490.3	0.36	0.70716 ± 1	0.70710
454A	64	459.1	0.40	0.70616 ± 2	0.70609
454B	85	474.6	0.51	0.70605 ± 3	0.70596

the basic part. The monzogranitic part has the lowest contents in HFS elements of all acid rocks in the complex; (d) The REE patterns of both parts are essentially parallel with much higher REE abundances in the basic part; (e) The Sr initial ratios of both parts are nearly identical.

Nevertheless, all these facts may be necessary but are not sufficient proofs for an origin by liquid immiscibility. There is still the possibility that all the acid veinlets had a similar origin. After their intrusions as foreign liquids into microdioritic magmas, mixing between the contrasted magmas was prevented due to high viscosities, but some equilibration by crossed-diffusion was possible in the case of the pair 454 B/A. Because the mass ratio A/B is small, only the acid component will be depleted in HFS elements by such a process. Tables 4 and 5 show indeed that the microdiorite 454 B is not particularly enriched in HFS elements with respect to the other microdiorites and that the acid veinlet 454 A has the lowest contents of HFS elements of all the granodioritic to granitic samples.

We conclude, that the process of unmixing due to liquid immiscibility is a viable but certainly not unique model

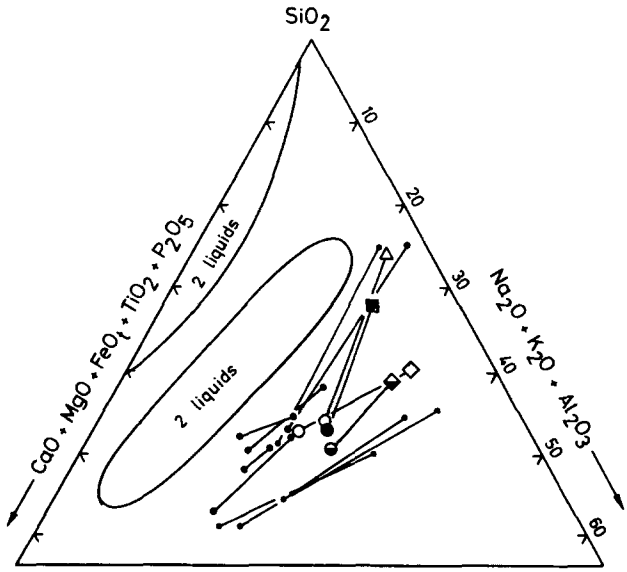

Fig. 10. Greig diagram showing field of liquid immiscibility in the system leucite-fayalite-SiO_2, tielines for the four basic/acid pairs of this study (symbols as in Fig. 4), and tielines for various conjugate volcanic rocks for which an origin by liquid immiscibility has been suggested (small points; Roedder 1979: Fig. 2–8C

to explain the origin of the monzodiorite/monzogranite pairs in the net-veined parts of the dikes. To accept this model means to accept the coexistence on a small scale, i.e., even in the same dike, of net-veined parts of completely different origins. From another point of view, one could state, that an origin of the pair 454 B/454 A by unmixing due to liquid immiscibility cannot be disproved but has to be considered as unlikely.

Acknowledgments. Financial support by the Deutsche Forschungsgemeinschaft (OK 2/24-1, Al 166/4) is gratefully acknowledged. Thanks are due to Georgios Katisikatsos (I.G.M.E., Athens) for introducing M.O. to the geology of Samos during a joint field trip in 1981 and to Jana Stepanek, Werner Sauerschell, and Georg Okrusch for assistance during the field work. We are indebted to Annerose Walk, Marion Kappler, Roland Gehann, Frank Volker, Udo Karch (Karlsruhe), Otto Ewald (Braunschweig), and Rosemarie Baur (Würzburg) for carrying out bulk rock analyses. Microprobe facilities were kindly provided by Joachim Huth (MPI für Chemie, Mainz) and Martin Olesch (Würzburg). Bernd Jünger (Krebsforschungszentrum Heidelberg) carried out the irradiation for the INAA determinations. Horst Klappert, Margot Metz, Annedore Reimann, Lutz Thiesswald, and Detlef Uebersohn (BRG Hannover) contributed to the K–Ar analyses. Bent Hansen, Boris Grauert, Ulrich Kramm, and Albrecht Baumann (ZLG Münster) gave valuable advice for the Rb–Sr isotope determinations. Klaus-Peter Kelber (Würzburg) accomplished some of the line drawings, Elke Weiher (Karlsruhe) did the photographic reductions of the figures, and Gabi Baumann (Karlsruhe) typed the manuscript. Thanks are further due to W.E. Stephens, J. Hoefs, and an unknown reviewer for their constructive criticisms of the first version of this paper.

References

Altherr R (1981) Zur Petrologie der miozänen Granitoide der Zentralägäis (Griechenland). Dr. habil Thesis, Univ Braunschweig

Altherr R, Kreuzer H, Wendt I, Lenz H, Wagner GA, Keller J, Harre W, Höhndorf A (1982) A late Oligocene/Early Miocene High Temperature Belt in the Attic-Cycladic Crystalline Complex (SE Pelagonian, Greece). Geol Jahrb E23:97–164

Altherr R, Henjes-Kunst F, Matthews A (1984) Primäre Sr- und O-Isotopenzusammensetzungen von miozänen I-Typ-Granitoiden der Zentralägäis und daraus abgeleitete Rahmenbedingungen für Modelle zur Genese dieser Gesteine. Fortschr Mineral 62 1:8

Ayranci B (1977) The major-, minor-, and trace-element analysis of silicate rocks and minerals from a single sample solution. Schweiz Mineral Petrogr Mitt 57:299–312

Bender JF, Hanson GN, Bence AE (1982) The Cortlandt complex: evidence for large-scale liquid immiscibility involving granodiorite and diorite magmas. Earth Planet Sci Lett 58:330–344

Blake DH (1966) The net-veined complex of the Austurhorn intrusion, southeastern Iceland. J Geol 74:891–907

Bowen NL (1928) The Evolution of Igneous Rocks, Princeton Univ Press, Princeton

Butz J (1912) Die Eruptivgesteine der Insel Samos. Centralbl Min 1912:609–615, 641–651, 673–683

Eby GN (1979) Mount Johnson, Quebec – An example of silicate-liquid immiscibility? Geology 7:491–494

Foster MD (1960) Interpretation of the Composition of Trioctahedral Micas. US Geol Surv Prof Pap 345-B:11–49

Fourcade S, Allègre CJ (1981) Trace Elements Behaviour in Granite Genesis: A case study. The Calc-Alkaline Plutonic Association from the Querigut Complex (Pyrénées, France). Contrib Mineral Petrol 76:177–195

Halliday AN, Stephens WE, Harmon RS (1980) Rb–Sr and O isotopic relationships in 3 zoned Caledonian granitic plutons, Southern Uplands, Scotland: evidence for varied sources and hybridization of magmas. J Geol Soc London 137:329–348

Leake BE (1978) Subcommittee on amphiboles: nomenclature of amphiboles. Mineral Mag 42:533–563

Mezger K, Okrusch M (1985) Metamorphism of the variegated sequence at Kallithea, Samos, Greece. Tschermaks Mineral Petrogr Mitt (in press)

Nockolds SR (1947) The relation between chemical composition and paragenesis in the biotite micas of igneous rocks. Am J Sci 245:401–420

Otto J (1974) Die Einschlüsse im Granit von Oberkirch (Nordschwarzwald). Ber Naturforsch Ges Freiburg i Br 64:83–174

Papanikolaou D (1979) Unités tectoniques et phases de déformation dans l'ile de Samos, Mer Egée, Grèce. Bull soc Géol France (7) 21:745–752

Peters A (1968) Ein neues Verfahren zur Bestimmung von Eisen-II-oxid in Mineralen und Gesteinen. N Jahrb Miner Monatsh 1968:119–125

Philipson A (1959) Die griechischen Landschaften. Das Aegaeische Meer und seine Inseln. Klostermann Frankfurt

Philpotts AR (1972) Density, surface tension, and viscosity of the immiscible phase in a basic, alkaline magma. Lithos 5:1–18

Philpotts AR (1976) Silicate liquid immiscibility: Its probable extent and petrogenetic significance. Am J Sci 276:1147–1177

Philpotts AR, Hodgson CJ (1968) Role of liquid immiscibility in alkaline rock genesis. 23rd Intern Geol Congr Prague Proc 2:175–188

Reid JB, Evans OC, Fates DG (1983) Magma mixing in granitic rocks of the central Sierra Nevada, California. Earth Planet Sci Lett 66:243–261

Robert U, Cantagrel JM (1977) Le volcanisme basaltique dans le Sud-Est de la Merd' Egée. Données géochronologiques et relations avec la tectonique. In: Kallergis (ed) "Proceedings of the VI Colloquium on the Geology of the Aegean Region, Athens," pp 961–867, I.G.M.E. Athens

Roedder E (1979) Silicate liquid immiscibility in magmas. In: Yoder (ed) "The Evolution of the Igneous Rocks, 50th Anniversary Perspectives", Princeton Univ Press Princeton

Ryerson FJ, Hess PC (1978) Implications of liquid-liquid distribution coefficients to mineral-liquid partitioning. Geochim Cosmochim Acta 42:921–932

Seidel E, Kreuzer H, Harre W (1982) A Late Oligocene/Early Miocene High Pressure Belt in the External Hellenides. Geol Jahrb E23:165–206

Streckeisen A (1976) To each plutonic rock its proper name. Earth-Sci Rev 12:1–33

Taylor TR, Vogel TA, Wilband JT (1980) The composite dikes at Mount Desert Island, Maine: an example of coexisting acid and basic magmas. J Geol 88:433–444

Theodoropoulos D (1979) Geological map of Greece, 1:50.000, Samos Island. I.G.M.E. Athens

Vogel TA, Wilband JT (1978) Coexisting acidic and basic melts: geochemistry of a composite dike. J Geol 86:353–371

Walker GPL, Skelhorn RR (1966) Some associations of acid and basic igneous rocks. Earth-Sci Rev 2:93–109

Watson EB (1976) Two liquid partition coefficients. Experimental data and geochemical implications. Contrib Mineral Petrol 56:119–134

Wiebe RA (1973) Relations between coexisting basaltic and granitic magmas in a composite dike. Am J Sci 273:130–151

Wiebe RA (1974) Coexisting intermediate and basic magmas, Ingonish, Cape Breton Island. J Geol 82:74–87

Wiebe RA (1979) Fractionation and liquid immiscibility in an anorthositic pluton of the Nain Complex, Labrador. J Petrol 20:239–269

Wiebe RA (1980) Commingling of contrasted magmas in the plutonic environment: examples from the Nain anorthositic complex. J Geol 88:197–209

Wiebe RA, Wild T (1983) Fractional crystallization and magma mixing in the Tigalak layered intrusion, the Nain anorthosite complex, Labrador. Contrib Mineral Petrol 84:327–344

Yoder HSJr (1973) Contemporaneous basaltic and rhyolitic magmas. Am Mineral 58:152–171

Received December 4, 1984 / Accepted April 6, 1985